8-2018

Optimized Angles of the Swing Hyperspectral Imaging Tower for Single Corn Plant

Libo Zhang
Purdue University

OPTIMIZED ANGLES OF THE SWING HYPERSPECTRAL IMAGING TOWER FOR SINGLE CORN PLANT

A Dissertation

Submitted to the Faculty

of

Purdue University

by

Libo Zhang

In Partial Fulfillment of the

Requirements for the Degree

of

Master of Science in Agricultural & Biological Engineering

August 2018

Purdue University

West Lafayette, Indiana

THE PURDUE UNIVERSITY GRADUATE SCHOOL

STATEMENT OF DISSERTATION APPROVAL

Dr. Jian Jin, Chair

Department of Agricultural and Biological Engineering

Dr. Dennis R. Buckmaster

Department of Agricultural and Biological Engineering

Dr. Dharmendra Saraswat

Department of Agricultural and Biological Engineering

Approved by:

Dr. Bernard A. Engel

Head of the Departmental Graduate Program

For my parents, younger brother and sister-in-law, who support me to study abroad, and particularly for my little niece, who recently joined our family and brought a lot of happiness.

For my friends and tutors, Kailiang Zhang in China Agricultural University and Jun Li in Beijing Union University, who encouraged me to pursue decent education and study in Agricultural & Biological Engineering Department, Purdue University.

ACKNOWLEDGMENTS

First of all, I must express the gratitude to my supervisor, Dr. Jian Jin, for his inspiring vision into this tilted imaging angle project and continuous supports through the entire experimental processing. Dr. Jin is enthusiastic and passionate, leading me to locate the problems during experimental preparation and data analysis. I was strongly impressed by his capacities of expression and communication, which always make his ideas and thoughts explicit to students like me. I wish I could learn more from him and affect my friends and colleagues with these kinds of abilities.

Secondly, I'd like to thank Dr. Michael V Mickelbart and Michael J Gosney in Horticulture and Landscape Architecture, who provided a lot of help when growing experimental samples (corn plants) in the Horticulture greenhouse. They're professional and trained me how to control different treatments using different concentrations of fertilizers. Thanks to their selfless help, I completed the experiments with good-quality experimental samples.

Also, I'd like to thank Scott Brand, the manager of machine shop facility, for his selfless help when I assembled the swing hyperspectral imaging tower in the ADM building. Many times, Scott machined the aluminum extruder parts for me,

and provided various categories of tools to help complete the whole setup. Many of his suggestions helped me make the swing tower more steady and secure to use.

Finally, I appreciate the time my colleagues spent to discuss with me and help me determine the methods of experimental design and data analysis. They're so nice that I always walk over to them whenever I need more hands during the experimental processing. I'll manage to return all of them as the way I was treated in the study and daily life.

TABLE OF CONTENTS

Page

LIST OF TABLES

LIST OF FIGURES

ABBREVIATIONS

abbr	abbreviation
NDVI	Normalized Difference Vegetation Index
SIPI	Structure Insensitive Pigment Index
RWC	Relative Water Content
NRI	Nitrogen Reflectance Index
TLA	Total Leaf Area
ALA	Average Leaf Angle
N	Nitrogen
PLSR	Partial Least Square Regression
LAI	Leaf Area Index
ppm	Parts Per Million
PVC	Polyvinyl Chloride
SPAD	Soil Plant Analysis Development
NIR	Near Infrared

ABSTRACT

Zhang, Libo MS, Purdue University, August 2018. Optimized Angles of the Swing Hyperspectral Imaging Tower for Single Corn Plant. Major Professor: Jian Jin, Assistant Professor.

During recent years, hyperspectral imaging systems have been widely applied in the greenhouses for plant phenotyping purposes. Current imaging systems are mostly designed as either top view or side view imaging mode. Top-view is an ideal imaging angle for top leaves which are often more flat with more uniform reflectance. However, most bottom leaves are either blocked or shaded from top view. From side view, most leaves are viewable, and the entire structure can be imaged. However, at this angle most of the leaves are not facing the camera, which will impact the measurement quality. At the same time, there could be advantages with certain tilted imaging angle between top view and side view. Therefore, it's important to explore the impact of different imaging angles to the phenotyping quality. For this purpose, we designed a swing hyperspectral imaging tower which enables us to rotate the camera and lighting source to capture images at any angle from side view (0°) to top view (90°). 36 corn plants were grown and divided into 3 different treatments: high nitrogen (N) and well-watered (control group), high N and drought-stressed, and low N and well-watered. Each plant was imaged at 7 different angles from 0° to 90° with an interval of 15°. According to different treatments applied on experimental

samples, two comparative pairs were set up: drought-stressed group vs. control group (Pair 1); N-deficiency group vs. control group (Pair 2). In this study, normalized difference vegetation index (NDVI) and relative water content (RWC) were computed and compared to determine optimized imaging angle(s). For NDVI, the imaging angle near to top view is optimized to separate Pair 1, while, the imaging angle near to side view is optimized to distinguish Pair 2. For RWC, partial least square regression (PLSR) models were applied to predict pixel-level RWC distribution of each plant, and higher imaging angles (close to top view) are better to tell the RWC distribution difference in Pair 1. In conclusion, higher imaging angles (close to top view) are better to separate different water treatments, while, lower imaging angles (close to side view) are better to separate different N treatments.

1. INTRODUCTION

1.1 Plant phenotyping systems

Both DNA sequencing and precise quantification of plant traits are crucial for improving crop yields. An important task in the area of plant science is to understand how the connection performs between plant genotype and its phenotype (observable characteristics). Plant phenotyping techniques, thus, are utilized by researchers to explicate this correlation (Rahaman et al., 2015). Plant phenotyping is a comprehensive method to evaluate complicated plant traits such as growth, tolerance, morphology, physiology, biochemistry, ecology and yield (Li et al., 2014; Dhondt et al., 2013). During recent years, to provide quantitative analysis of plant features and accelerate progress in breeding for novel traits, plant phenotyping platforms have been widely applied in the growth chamber or greenhouse (Tester and Langridge, 2010; Fiorani and Schurr, 2013; Xiong et al., 2017).

These imaging platforms consist of hyperspectral cameras, artificial lighting source, mechanisms and computers, which work together to non-destructively capture plant traits under controlled conditions (Fahlgren et al., 2015; Klukas et al., 2014). PHENOPSIS (Granier et al., 2006) was developed to take images of Arabidopsis from top view to understand genotype-environment effects on plant growth. PhenoArch

(Sadok et al., 2007) is a phenotyping platform to capture images of a variety of species such as corn, wheat and sorghum under particular drought, temperature and light conditions, with cameras installed on the top view. GROWSCREEN (Walter et al., 2007; Nagel et al., 2012) integrates modern standard single-image processing procedures with an automated setup to rapidly acquire high-quality images of different plant species, and it focuses on the top-view imaging. Also, some breeding corporations, such as DuPont Pioneer and Monsanto, have developed automated plant phenotyping facilities in the greenhouse to analyze characteristics of corn, sorghum and other species from top view and side view.

From top view, more flat leaf surface can be imaged and reflectance intensity is more uniform. It's an ideal imaging angle for top leaves, but most bottom leaves are either blocked or shaded. In many cases, the bottom/lower leaves are more sensitive to environmental stresses, and show stress symptoms earlier than other leaves. From side view, we can obtain the entire structure of plants so that we're able to quantify leaves, plant heights and shoot areas (Hartmann et al., 2011). However, the leaves are not facing the side-view camera in most cases. The contents of several elements were found to be different among the margin, midrib and blade of a corn leaf (Sumner, 1977). For instance, the content of N in the midrib is less than that in the blade or margin. As a consequence, leaf biochemical contents might be inaccurately predicted based on side-view images. Both top view and side view imaging are imperfect. A tilted imaging angle could be a good compromise between them.

1.2 PROSAIL model

PROSAIL is a combination of PROSPECT (leaf optical properties model) and SAIL (canopy bi-directional reflectance model). At the leaf level, PROSPECT works on the simulation of directional-hemispherical reflectance of plants from 400 to 2500 nm (Jacquemoud and Baret, 1990; Schaepman-Strub et al., 2006; Jacquemoud et al., 2009). It uses two input variables: the leaf structure parameter (compact layers specifying the average amount of cell walls) and the leaf biochemical contents. At the canopy level, SAIL allows estimates of canopy architecture such as leaf area index (LAI) and leaf angle distribution by using bi-directional reflectance measurements. The bi-directional reflectance depends upon the direction of incident radiation and the direction from which the surface is being viewed.

PROSAIL has been widely used to simultaneously estimate the canopy biophysical/structural variables in agriculture and plant physiology due to its ease of use and general robustness (Salas and Henebry, 2014). In this study, the reflectance simulation in the range of 400 to 1000 nm, using the PROSAIL 5B package, was developed in Matlab R2016a software. The main input parameters (Table 1.1) include leaf structure parameter (N), chlorophyll content (C_{ab}), equivalent water thickness (C_w), dry matter content (C_m), brown pigments content (C_{bp}), leaf area index (LAI), average leaf angle ($LIDFa$), hot spot parameter (s_L), soil reflectance (ρ_s), ratio of diffuse to total incident radiation ($SKYL$), solar zenith angle (θ_s), viewing angle (θ_v), and relative azimuth angle (φ_{sv}). In this PROSAIL model, a standard corn plant uses the

Table 1.1.
Main variables of PROSAIL model including PROSPECT and SAIL

Model	Symbol	Quantity	Unit
PROSPECT	N	leaf structure parameter	–
	C_{ab}	chlorophyll a + b content	$\mu g{\cdot}cm^{-2}$
	C_w	equivalent water thickness	$g{\cdot}cm^{-2}$
	C_m	dry matter content	$g{\cdot}cm^{-2}$
	C_{bp}	brown pigments content	–
SAIL	LAI	leaf area index	–
	$LIDFa$	average leaf angle	deg
	s_L	hot spot parameter	–
	ρ_s	soil reflectance assumed Lambertian or not	–
	$SKYL$	ratio of diffuse to total incident radiation	–
	sza or θ_s	solar zenith angle	deg
	vza or θ_v	viewing zenith angle	deg
	raa or φ_{sv}	relative azimuth angle	deg

following parameters: $N = 1.518,\ C_{ab} = 58.0\ \mu g{\cdot}cm^{-2},\ C_w = 0.0131\ g{\cdot}cm^{-2},\ C_m = 0.003662\ g{\cdot}cm^{-2},\ C_{bp} = 0.0,\ LAI = 3.0,\ s_L = 0.01,\ \rho_s = 0,\ SKYL = 0.277$. To make the simulation as simple as possible, the solar zenith angle (θ_s), viewing zenith angle (θ_v) and relative azimuth angle (φ_{sv}) were all set as 0, which means the light-

ing source and camera face down on the top of the plants. Thus, only the average leaf angle ($LIDFa$) was changing in this model. There exist 4 different outputs: hemispherical-directional reflectance factor in viewing direction (rdot), bi-directional reflectance factor (rsot), directional-hemispherical reflectance factor for solar incident flux (rsdt), and bi-hemispherical reflectance factor (rddt). According to the introduction above, the bi-directional reflectance factor was picked and its spectra (Fig. 1.1) show that reflectance intensity changes a lot with the average leaf angle increasing. After normalizing the spectra, we found that there exist shape changes among spectra of different average leaf angles (Fig. 1.2). Then, normalized difference vegetation index (NDVI) was calculated to numerically exhibit the differences of 10 differential average leaf angles, and it decreases from 0.910 to 0.857 with the angle going up from 0 to 90 degrees (Fig. 1.3). If we rotate the camera and lighting source instead of the average leaf angle, imaging angle will affect the prediction of plant biochemical contents (e.g. NDVI).

1.3 Research objectives

According to the PROSAIL model, leaf reflectance spectra change at different imaging angles. However, current plant phenotyping systems only focus on side view or top view imaging mode. A tilted imaging angle could be a good compromise between them. Therefore, this research aimed to explore an optima between the side and top view imaging modes, and our objectives are listed below.

1. Design and build a swing hyperspectral imaging tower that enables us to capture images of plants at any angle from side view to top view

2. Grow corn plants in 3 different treatments (drought-stressed group, control group, and N-deficiency group), and image these plants with the designed swing hyperspectral imaging tower

3. Develop Matlab algorithms to process hyperspectral images, and determine optimized angles for NDVI and RWC indices by means of statistical analysis

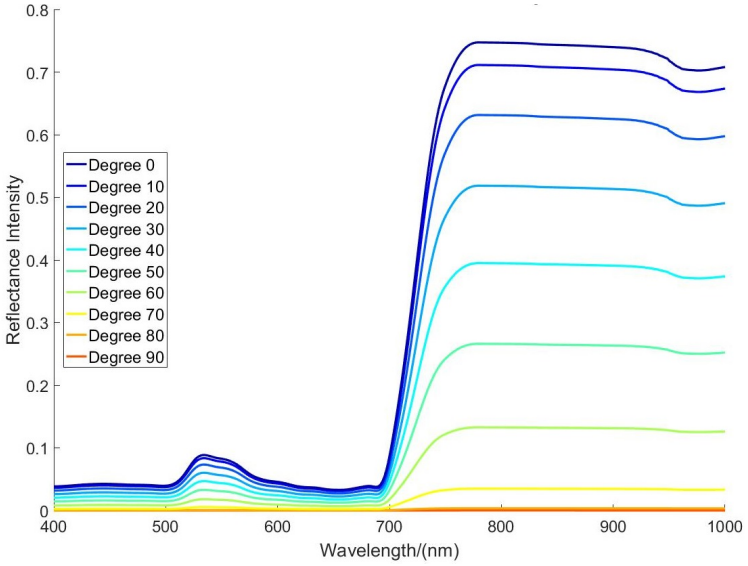

Fig. 1.1. Reflectance spectra of a standard corn plant with different average leaf angles (ALA) from the bi-directional PROSAIL model

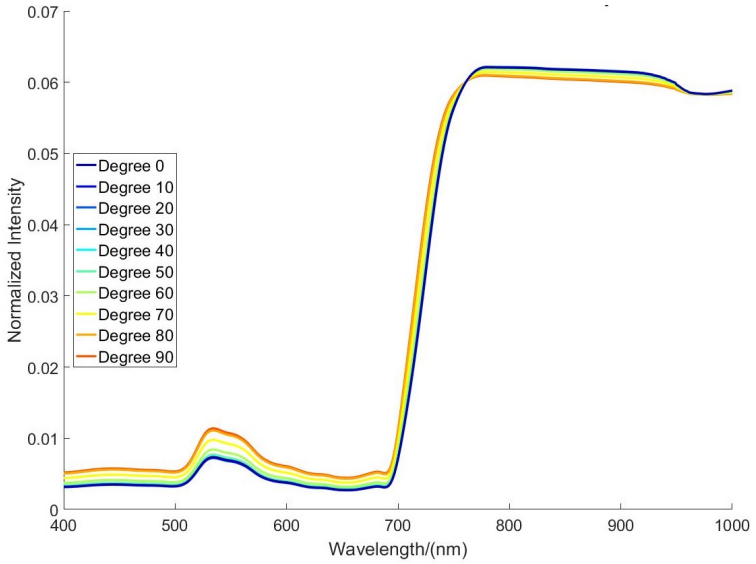

Fig. 1.2. Normalized reflectance spectra of a standard corn plant with different average leaf angles (ALA) from the bi-directional PROSAIL model

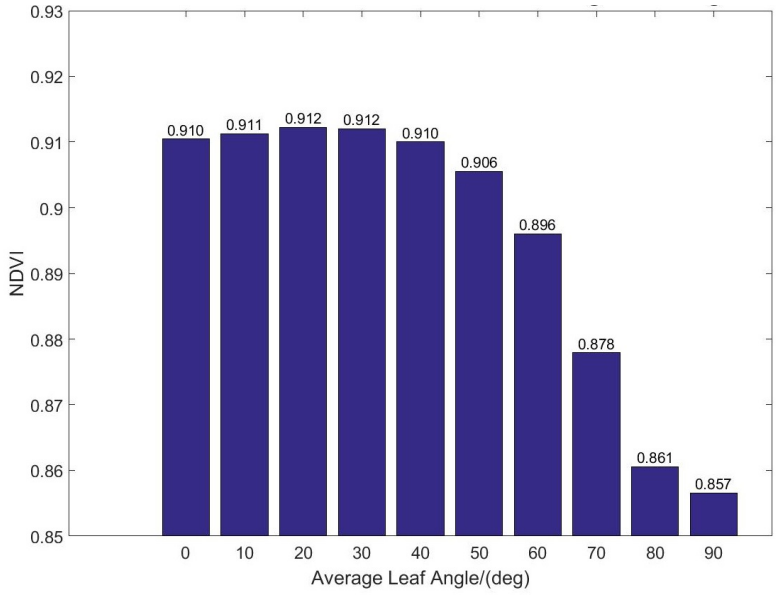

Fig. 1.3. Average normalized difference vegetation index (NDVI) of a standard corn plant with different average leaf angles (ALA) from the bi-directional PROSAIL model

2. MATERIALS AND METHODS

2.1 Hyperspectral imaging tower structure

To capture hyperspectral images from different viewing angles, a swing hyperspectral imaging tower was designed and built. It enables us to rotate the hyperspectral camera and lighting source to capture images of plants at any titled angle. This swing hyperspectral imaging system (Fig. 2.1) mainly consist of a line scanning hyperspectral camera (MSV-500 with mirror scanner, Middleton Spectral Vision Co., USA) with a 5.5 mega pixel sCMOS sensor, the assembled lighting source coupled with backlit halogen bulbs (MR16 GU10 Brushed Nickel, Lithonia Lighting Inc., USA), an angle detection sensor (MTi-300-AHRS, Xsens Technologies B.V., Netherlands) with roll/pitch static typical orientation errors of 0.2 degree, the rotating function components including winch, pulley, bearing and rod, and a Dell Precision Tower 5810 computer with the spectral imaging software (MSV.measure zyla mirrorscan, Middleton Spectral Vision Co., USA) used to adjust imaging parameters including integration time, frame rate, spectral resolution, image ROI, scanning start position, scanning end position, and scanning speed.

The hyperspectral camera (Fig. 2.2) is connected to the winch with the steel wire rope and supported by 40×40 mm aluminum extrusions on the bottom. When

Fig. 2.1. Structure of the swing hyperspectral imaging tower: outside and inside settings

(Top: outside; Bottom: inside)

(1. black cloth; 2. frame; 3. winch; 4. computer; 5. pulley; 6. steel rope; 7. light source; 8. rod and bearing; 9. corn plant; 10. rotating support)

taking images, only the two mirrors inside the mirror scanner move instead of the entire camera, which makes the system more stable. The MTi-300 sensor was fixed on the same surface with the camera to read pitch angles. A small fan was installed on the top of the camera to avoid overheating. The whole system was covered by Black Felt fabric to minimize the influence of ambient lights during the plant scanning. Also, the ground underneath the plants was covered by this fabric to minimize the impact of light reflectance on the floor.

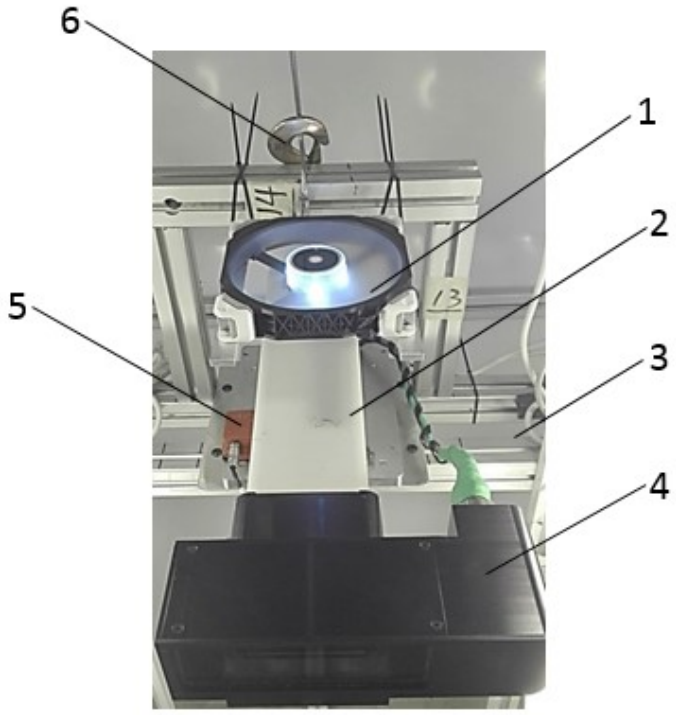

Fig. 2.2. Schematic of the hyperspectral camera installation in the swing hyperspectral imaging tower

(1. fan; 2. camera; 3. camera support frame; 4. mirror scanner; 5. MTi-300 sensor; 6. rope pothook)

2.2 Experimental samples

As described in Table 2.1, a total of 36 corn plants (genotype: Hybrid B73 x Mo17) were grown for this research. In the greenhouse, the lighting intensity, temperature and air flow velocity are distinct at different positions. For example, the region, closer to the air conditioner, has a lower temperature, leading to plants growing more slowly there. To reduce the effects of this so-called micro-environment in the greenhouse (Sharma et al., 1999), these corn plants were allocated in a randomized block design.

Table 2.1.
Summary table of experimental samples

Samples	corn plants		
Genotype	hybrid B73×Mo17		
Experiment design	randomized block design		
Growing location	horticultural greenhouse at Purdue		
Treatments	400 ppm N fertilizer	400 ppm N fertilizer	75 ppm N fertilizer
	well watered	drought stressed	well watered
Conditions	WW	WS	SW
Replicates	12	12	12
Stage	V8	V7	V8

Rates of fertilization are often given in parts per million (ppm) of N. Parts per million is a convenient unit of measurement for indicating the concentration of fertilizer solutions. It states the content of a fertilizer solution independent of the fertilizer analysis (Pimentel et al., 2005). The corn plants were divided into 12 blocks. In each block, there were 3 plants treated with 3 different treatments: 400 ppm N fertilizer and well-watered (control), 400 ppm N fertilizer and drought-stressed, and 75 ppm N fertilizer and well-watered. When irrigating, we guaranteed that each pot achieved saturation. Finally, the leaves of the drought-stressed plants were a little bit curling (Fig. 2.3); only the very bottom leaves of the N-deficiency plants started to become yellow (Fig. 2.4). In this study, leaf collar method was used to determine leaf stages of corn plants by counting the number of leaves with visible leaf collars. As Abendroth et al. described, the leaf collars are the light-colored and collar-like bands located at the base of exposed leaf blades, and theyre near the spots where the leaf blades contact with the stems of plants. This method starts with the lowest, short and round-tip true leaf, and ends with the uppermost leaf with a visible leaf collar. When imaged, the drought-stressed plants were at V7 stage, while, the well-watered plants were at V8 stage.

These corn plants were grown in the 9-inch-diameter and 8.75-inch-height plastic pots with the Fafard 52 mix soil. This soil source had a PH range of 5.5 to 6.5 and approximately contained 60% pine bark together with peat moss, perlite, vermiculite, dolomitic limestone and gypsum. The corn plants were sowed on October 17th, 2017 and imaged on November 28th, 2017, which indicates that the whole

Fig. 2.3. Two corn plants from the control group and drought-stressed group separately
(Left: control; Right: drought-stressed)

Fig. 2.4. Two corn plants from the control group and N-deficiency group separately
(Left: N-deficiency; Right: control)

growing period was 40 days. All the 36 corn plants were grown in the Horticulture greenhouse (40°25'16.2"N, 86°54'53.0"W) at Purdue University, West Lafayette, IN, USA.

2.3 Image acquisition

After finishing the assembly of the swing hyperspectral imaging tower, we executed a test. A corn plant was imaged at 11 different angles from side view (0°) to top view (90°). In Fig. 2.5, at 0°, the entire plant structure is visible, but the leaf blades cover a lot of view; at 90°, the leaf surface is more flat, but the bottom leaves are blocked or shaded by the top leaves; at a tilted angle, like 45° or 60°, we can see not only the entire plant structure (leaves and stem), but also more complete leaf surface (blade, margin and midrib).

When both the imaging tower and experimental samples were ready, we started the formal experiment. To finish the experiment in one day, 7 imaging angles were picked from side view to top view with an interval of 15 degrees. Before imaging, a variety of parameters of the hyperspectral imaging device were calibrated (Table 2.2). First of all, the camera focusing was adjusted to the optima to guarantee the high quality of images. And then, the integration time (12 milliseconds), frame rate (50 fps), scanning start position (12 degrees) and scanning end position (-11.1 degrees) were determined according to the size of the largest plant. To decrease the dimensions of images and save storage space, the spectral binning (×2) was applied. The optical

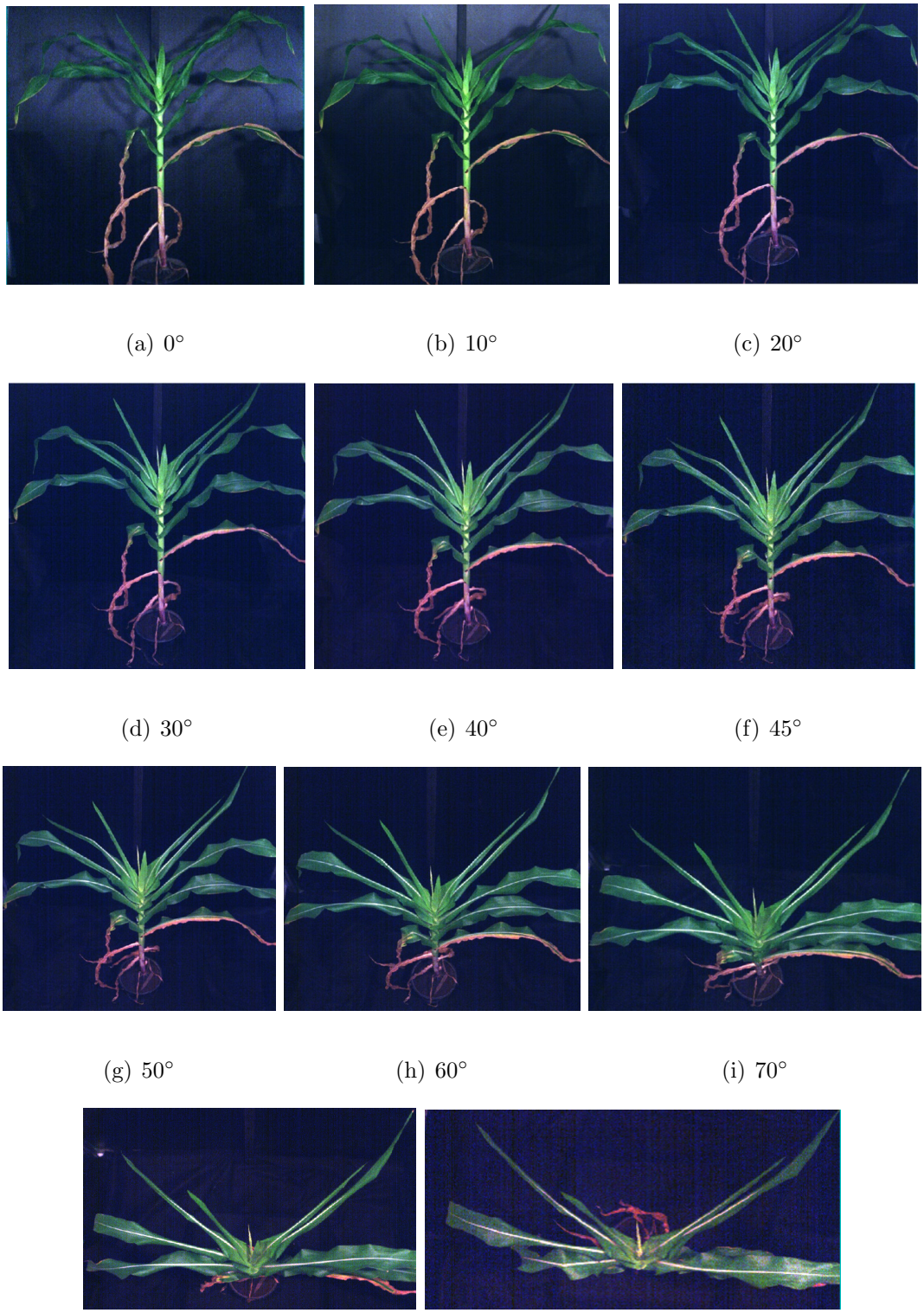

(a) 0° (b) 10° (c) 20°

(d) 30° (e) 40° (f) 45°

(g) 50° (h) 60° (i) 70°

(j) 80° (k) 90°

Fig. 2.5. Showcase images of a corn plant at 11 different imaging angles from side view to top view

resolution was approximately 1.22∼1.33 nm, and there were 500 bands in the spectral range of 380∼1017 nm. The plants were allocated 2.3 meters away from the camera lens, and their center heights roughly equaled to the rotating pivot, which ensured the distance between the plants and camera lens consistent at different imaging angles.

At the beginning, the swing imaging tower was set at side view (0°), and 36 corn plants were put inside the tower and scanned one by one in the order of drought-stressed group, control group and N-deficiency group. Compared with imaging each plant at all angles before the next plant, this prevented the corn plants from staying inside the hot tower for too long time. After 0° imaging was done, the hyperspectral camera was adjusted to 15° using the hand winch, and all the plants were imaged again in the same order. This cycle was repeated until top view (90°) imaging was completed. At last, all the 36 corn plants were imaged at 7 different angles from side view to top view with an interval of 15°. A polyvinyl chloride (PVC) panel was scanned as white balance to calibrate the images. The objective of the white balance calibration was to minimize the effects of the uneven intensity of the lighting source in different bands.

The whole experiment was completed in the workshop environment (40°41'63.6"N, 86°91'97.1"W) where the steady indoor temperature (20°C) helped us minimize the impacts to plants of changing temperature during the imaging work.

Table 2.2.
Specifications of the hyperspectral camera for image acquisition

Parameters	**Corresponding settings**
Camera model	ZYLA-5.5-USB3
Gain mode	12-bit (low noise)
Shutter mode	rolling
Readout rate	280 MHz
Spatial binning	×1
Spectral binning	×2
Spectral range	380−1017 nm
Optical resolution	1.22-1.33 nm
Integration time for plants	12 ms
Integration time for white balance	7.7 ms
Frame rate	50 fps
Scan start position	12 *deg*
Scan end position	-11.1 *deg*
Image spatial dimension	1848×2204 (samples×lines)
Image Spectral dimension	500 (bands)
Distance between lens and plants	2.3 meters

2.4 Ground truth measurements

To provide references to data analysis, ground truth measurements were conducted after imaging. The measurements mainly contained soil plant analysis development (SPAD), relative water content (RWC), leaf nitrogen content, and fresh and dry weights. Methods to take and calculate these indices are introduced below.

2.4.1 Soil plant analysis development

The soil plant analysis development (SPAD), which indicates relative chlorophyll content, is widely used by researchers and farmers all over the world, and the SPAD-502Plus meter was designed to help users improve crop quality by providing an indication of the amount of chlorophyll content in the leaves of plants (Reyes et al., 2017). The chlorophyll content can be used to determine the healthy conditions of plants. The SPAD-502Plus tells the relative chlorophyll concentration by measuring the leaf absorbance in the red and near-infrared bands (Pagola et al., 2008), which means SPAD values are relative numbers without units. In this study, the SPAD-502Plus meter was utilized to measure chlorophyll contents of top-collared leaves on each of which 3 spots were measured (Yuan et al., 2016).

In the box plot of average SPAD values of top-collared leaves (Fig. 2.6), for Pair 1, the control group always has higher values than the drought-stressed group, which indicates drought stress leads to less chlorophyll content in the leaves; meanwhile, for Pair 2, the control group has much higher values than the N-deficiency

group, which means the N-deficiency treatment causes much less chlorophyll content in the leaves.

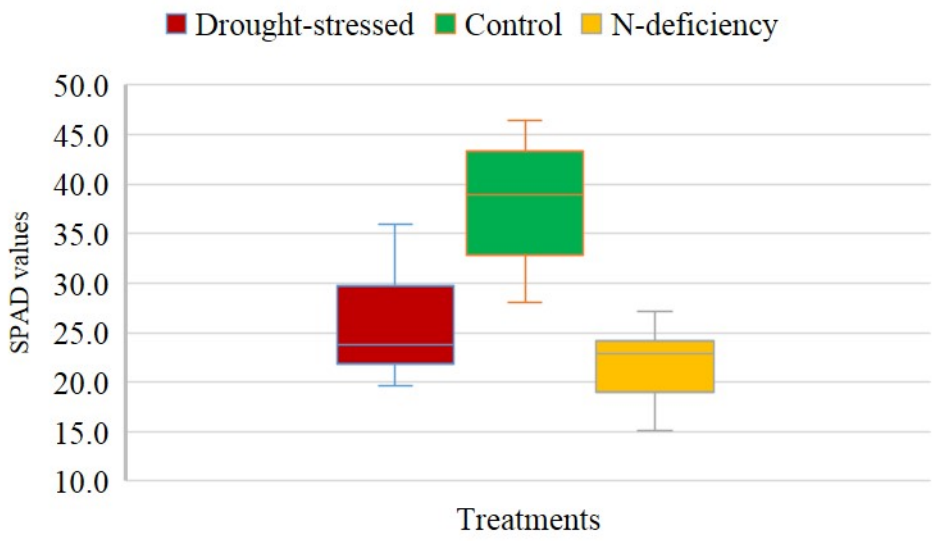

Fig. 2.6. Box plot of average SPAD values of top-collared leaves in 3 different treatments

2.4.2 Relative water content

Relative water content (RWC) is an appropriate measure of plant water status in terms of the physiological consequence of cellular water deficit. In this study, a simple but widely-used measure method was applied. It estimates the ratio of the current water content of the leaf sample to the maximum water content it can hold at full turgidity (Turner, 1981; Matin et al., 1987). In other words, it measures water deficit in the leaf sample. Generally, the RWC ranges between 98% in the turgid leaves and 40% in the severely drought leaves.

After SPAD measurement, a piece of leaf sample on the top-collared leaf of each plant was cut off and weighed to obtain leaf sample weight (W). The samples, then, were immediately hydrated to full turgidity under the normal room lighting and temperature. About 8 hours later, the surface humidity on the leaf samples were well dried lightly and quickly with the filter paper. And then, the samples were weighed to get the fully turgid weight (TW). At last, the leaf samples were put inside the dry oven (persistently at 60°C) for approximately 24 hours to obtain the dry weight (DW). All the weights were recorded with four decimals after gram (g). The RWC was calculated by the formula (eq. 2.1) below:

$$RWC(\%) = [(W - DW)/(TW - DW)] \times 100\% \tag{2.1}$$

where, $W-$ sample fresh weight

$TW-$ sample turgid weight

$DW-$ sample dry weight

From the box plot of RWC of top-collared leaves in 3 different treatments (Fig. 2.7), the control group has much higher values than the drought-stressed group, while, the N-deficiency group has a little bit higher values than the control group.

2.4.3 Leaf nitrogen content

To measure leaf nitrogen contents, we cut top-collared leaves off, and then put them in the dry oven (persistently at 60°C) for at least one week until their weights

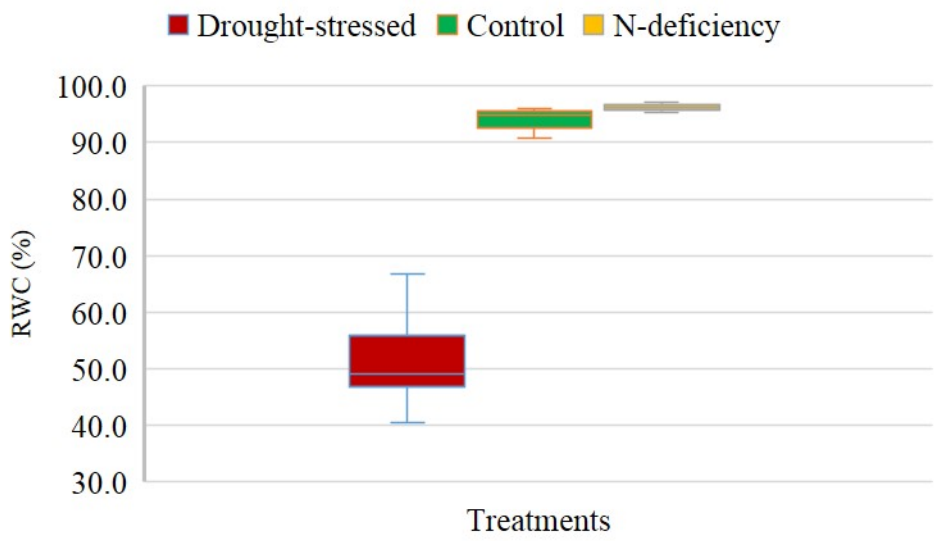

Fig. 2.7. Box plot of RWC of top-collared leaves in 3 different treatments

were constant. The dry leaf samples were pounded to powders transferred to labeled test tubes later. In this thesis, the Thermo Scientific FlashEA 1112 Nitrogen and Carbon Analyzer for Soils, Sediments and Filters (CE Elantech, Lakewood, NJ, USA) was used as the N analyzer. The FlashEA 1112 is based upon oxidation of samples by "flash dynamic combustion" which converts organic and inorganic substances into combustion gases. In the analyzer, N and carbon enter a chromatographic column and then to a thermal conductivity detector that generates electrical signals. At last, the percentage of N and carbon was recorded as leaf N content.

In the box plot of leaf nitrogen contents of top-collared leaves in different treatments(Fig. 2.8), when comparing the drought-stressed group and control group (Pair 1), we found that the former has a little bit higher values than the latter, which

indicates drought-stressed leaves contain higher N percentage than well-watered leaves under the same N concentration of fertilizers; meanwhile, in Pair 2, the control group has much higher leaf nitrogen contents than the N-deficiency group, which means the N-deficit leads to less N percentage over carbon in the top-collared leaves.

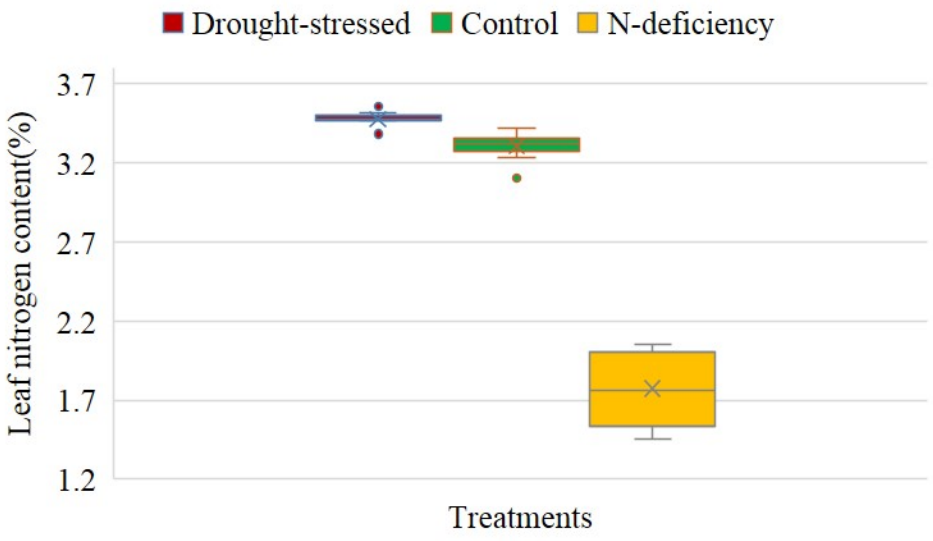

Fig. 2.8. Box plot of leaf nitrogen contents of top-collared leaves in 3 different treatments

2.4.4 Fresh and dry weight

At the end of this experiment, all the plants including leaves and stems were cut down at the position close to root, and then weighed to record fresh weights. Later on, they were put into the dry oven (persistently at 60°C) to obtain dry weights. The dry weights can be referred as biomass of plants.

From the box plots of fresh and dry weights of plants in different treatments (Fig 2.9 & Fig. 2.10), the control group always has the highest fresh and dry weights, while, the drought-stressed group always has the lowest fresh and dry weights. The drought stress severely impacts the growth of plants. Although the N deficit also affects the accumulation of biomass in the plants, it's not so severe as the drought stress does.

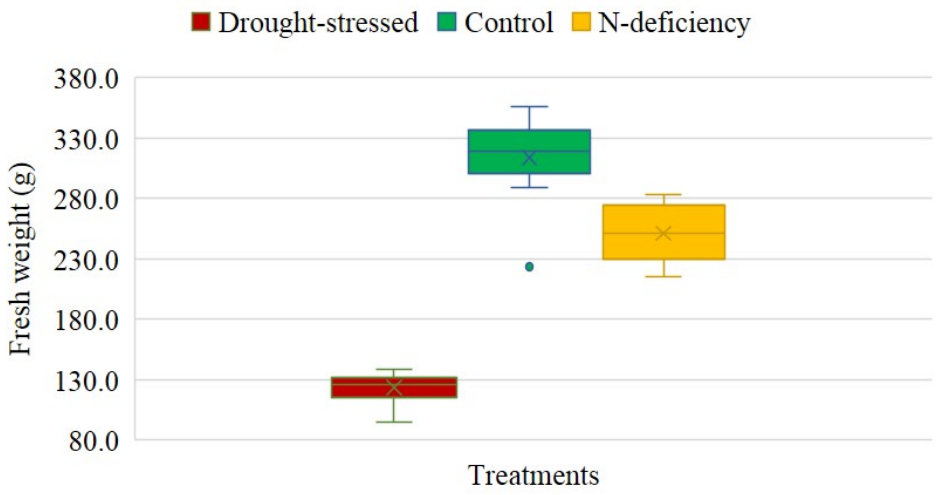

Fig. 2.9. Box plot of fresh weights of plants (leaves and stems) in 3 different treatments

2.5 Image segmentation

To obtain morphological properties of plants and analyze their spectra, we have to segment the plants out of the background. Matlab algorithm utilizing the "red edge" region (in this study, we used 680 to 732 nm) was developed to achieve this goal. The red edge region contains high information in the vegetation spectra, caused

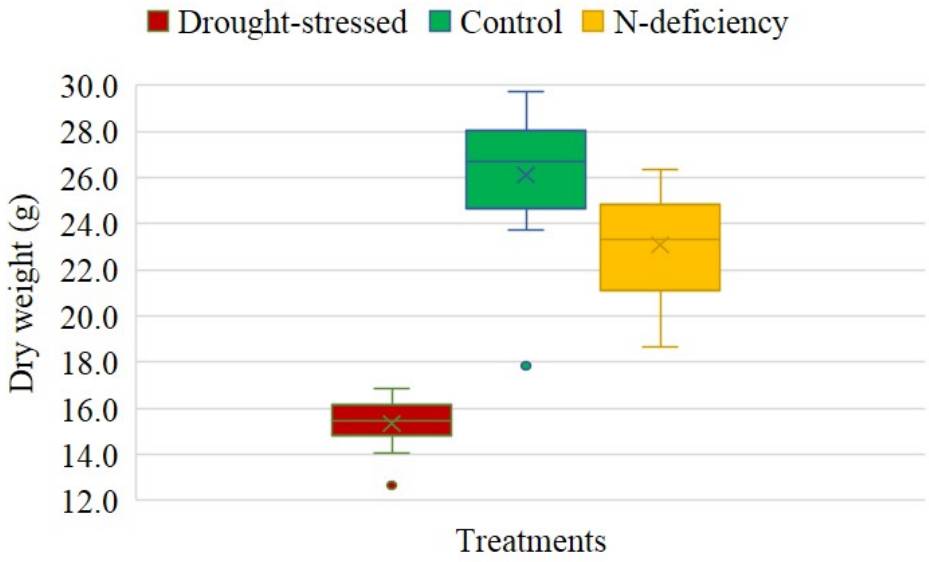

Fig. 2.10. Box plot of dry weights of plants (leaves and stems) in 3 different treatments

by the combined effects of strong chlorophyll absorption in the red wavelengths and high reflectance in the near-infrared (NIR) wavelengths (Collins, 1978; Elvidge and Chen, 1995).

In most cases, the reflectance intensity of plants extremely goes up in the red-edge region, while, the reflectance intensity of the background decreases in this range. As a consequence, there exist two different characteristic curves, whose tails end up with significant discrimination, but their centers intersect. To enlarge the difference at the tails and minimize the impact of crossover in the middle, the convolution methodology was applied, and a vector of integers from -20 to 20 were multiplied to the reflectance intensity vector in the red-edge region. Below is the kernel of this hyperspectral image segmentation algorithm:

$lin = transpose(-20:20);$

$convolution = lin' * transpose(squeeze(img(:,:,I_{680}:I_{732})))/(lin' * lin);$

$seg = convolution > threshold;$

Where, *lin* stands for the integer vector multiplied to reflectance intensity vector in the red-edge region; *convolution* means the result after multiplication; *plant* indicates the segmentation result after using threshold.

In this study, 7 was picked as the threshold for corn plants, above which are plant pixels, while, behind which are pixels belonging to the background. The morphological operation "bwareaopen" was subsequently applied to obtain optimizing segmentation results. In Fig. 2.11, the segmentation results of a corn plant at different imaging angles are illustrated. After segmentation, we can exact many kinds of morphological traits such as total leaf area (TLA), major axis length, minor axis length, eccentricity, solidity and convex area. Furthermore, we can utilize spectra of plants to directly compute various indices such as normalized difference vegetation index, nitrogen reflectance index (NRI) and structure insensitive pigment index (SIPI), and to indirectly predict relative water content (RWC) through building statistical models. In this thesis, we focus on NDVI and RWC indices to compare different imaging angles from side view to top view.

(a) 0° (b) 15° (c) 30°

(d) 45° (e) 60°

(f) 75° (g) 90°

Fig. 2.11. Binary images for segmentation results of a corn plant at different imaging angles from side view to top view with an interval of 15°

3. RESULTS AND DISCUSSION

3.1 NDVI

The normalized difference vegetation index (NDVI) is a standardized index allowing us to display the greenness of plants (Jackson et al., 1983). It takes advantage of the contrast of chlorophyll's high absorption in the red band and its high reflectivity in the near-infrared (NIR) band. Generally, in the NIR band, healthy leaves display higher reflection than the N-deficiency or diseased leaves do; while, in the visible band, healthy leaves reflect less than the N-deficiency or diseased leaves do. The reflection differences in the red and NIR bands enable us to monitor the greenness or chlorophyll pigment content in the leaves (Enciso et al., 2017). Moreover, NDVI can be used to estimate leaf water content and other physiological variables (Tucker, 1979). NDVI is calculated on the pixel basis as the normalized difference between the red and NIR bands (eq. 3.1):

$$NDVI = \frac{NIR - RED}{NIR + RED} \tag{3.1}$$

Where, NIR is the reflectance intensity of near-infrared band, and RED is the reflectance intensity of red color band. As described by Behmann et al., 800 nm was picked as NIR, and 680 nm was selected as RED.

3.1.1 Plant level

In TIBCO Spotfire, the data visualization and analytics software, the box plot of averaged NDVI through all the pixels on each plant (plant-level NDVI) in 3 treatments at different imaging angles was generated (Fig. 3.1). For the control group, NDVI values slightly go up with the imaging angle increasing, while, for the N-deficiency group, the values extremely rise with the angle increasing especially at the lower imaging angles. However, the drought-stressed group presents a different trend, NDVI values increasing at the beginning, decreasing later on, and increasing again at last. The control group always has higher NDVI values than the other two groups. Because during vegetative growth, both the drought stress and N deficiency significantly decrease chlorophyll a, chlorophyll b and total chlorophyll content (Lei et al., 2006; Baresel et al., 2017).

To see which imaging angle(s) discriminate Pair 1 and Pair 2 most significantly, the t-test was applied, and p-values were computed for different imaging angles. The t-test analyzes the means of two populations, and is commonly used to test the difference between the samples with small sizes. From the bar chart of t-test result of plant-level NDVI in two comparative pairs at different imaging angles (Fig. 3.2), x-axis stands for imaging angles from side view to top view, and y-axis means -log($p-value$). Thus, the difference is bigger when the y-axis value is larger. For the drought-stressed group and control group (Pair 1), the difference is becoming larger

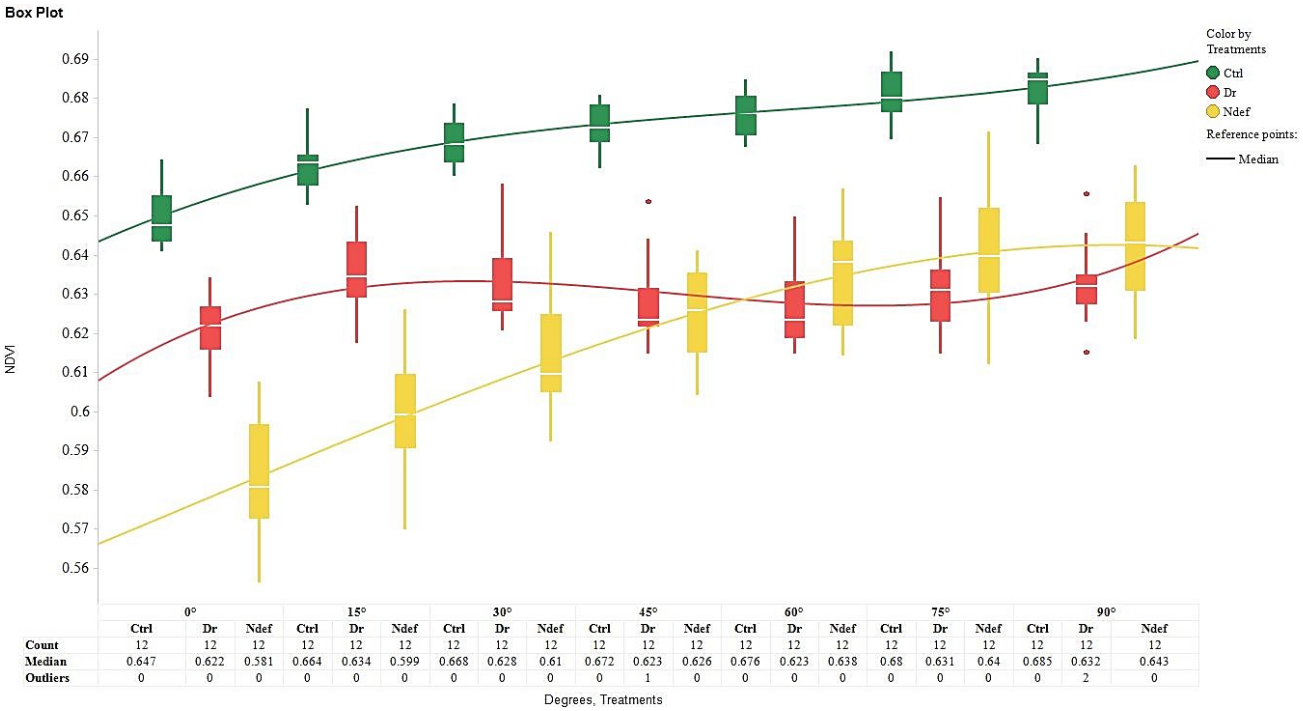

	0°			15°			30°			45°			60°			75°			90°		
	Ctrl	Dr	Ndef	Ctrl	Dr	Ndef	Ctrl	Dr	Ndef	Ctrl	Dr	Ndef	Ctrl	Dr	Ndef	Ctrl	Dr	Ndef	Ctrl	Dr	Ndef
Count	12	12	12	12	12	12	12	12	12	12	12	12	12	12	12	12	12	12	12	12	12
Median	0.647	0.622	0.581	0.664	0.634	0.599	0.668	0.628	0.61	0.672	0.623	0.626	0.676	0.623	0.638	0.68	0.631	0.64	0.685	0.632	0.643
Outliers	0	0	0	0	0	0	0	0	0	0	1	0	0	0	0	0	0	0	0	2	0

Fig. 3.1. Box plot of averaged NDVI through all the pixels on each plant (plant-level NDVI) in 3 treatments at different imaging angles from side view to top view
(Note: Ctrl means the control group, Dr means the drought-stressed group, and Ndef means the N-deficiency group.)

at higher imaging angles; meanwhile, for the N-deficiency group and control group (Pair 2), the difference is becoming larger at lower imaging angles.

3.1.2 Pixel level

Averaged NDVI through all the pixels on one plant doesnt take into account the stress distribution across the plant. To explore the difference in stress distribution, NDVI value of each pixel was calculated with the same formula (eq. 3.1), and the

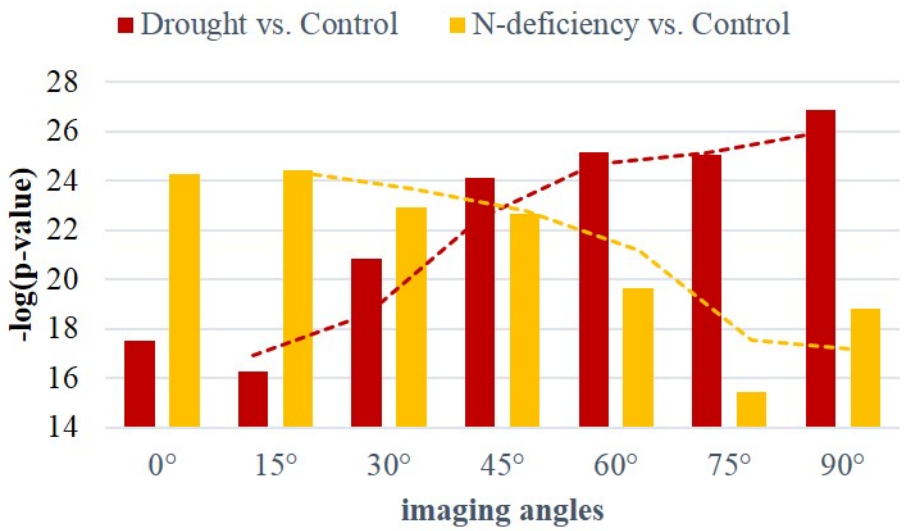

Fig. 3.2. Bar chart of t-test result of averaged NDVI through all the pixels on each plant (plant-level NDVI) in 2 comparative pairs at different imaging angles from side view to top view

colormaps of NDVI distributions on the whole plants were generated. In Fig. 3.3, warmer colors refer to for high NDVI values, while, colder colors refer to low NDVI values. Generally, the top leaves contain more chlorophyll, so they display more redness than bottom leaves. The control plant always exhibit more redness than the other two plants at all the imaging angles. The shooting area and height of the drought-stressed plant are smaller than plants in the other two treatments. The N-deficiency plant display more blueness on the very bottom leaves and leaf collars, but the blueness is gradually blocked by top leaves, and the difference between the N-deficiency and control plants becomes smaller at higher imaging angles; however, the difference between the drought-stressed and control plants becomes larger at higher imaging angles.

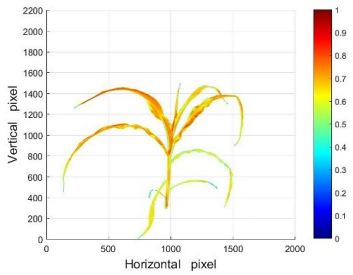

(a) 0°-drought

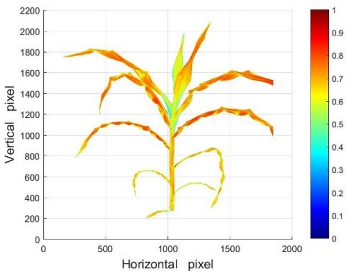

(b) 0°-control

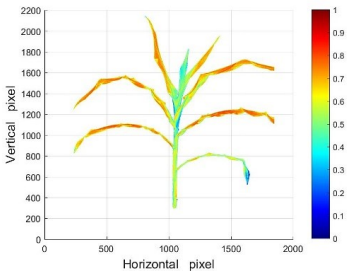

(c) 0°-N-deficiency

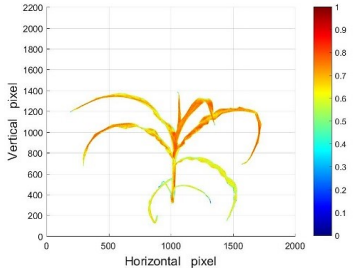

(d) 15°-drought

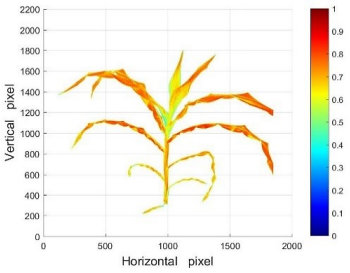

(e) 15°-control

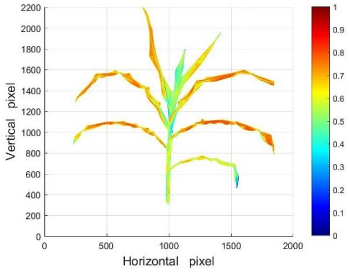

(f) 15°-N-deficiency

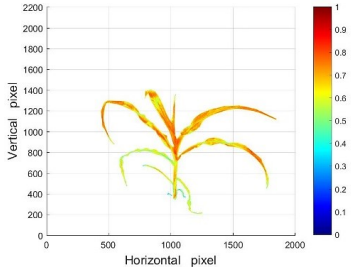

(g) 30°-drought

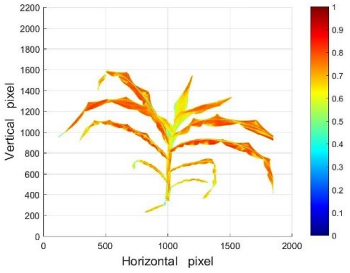

(h) 30°-control

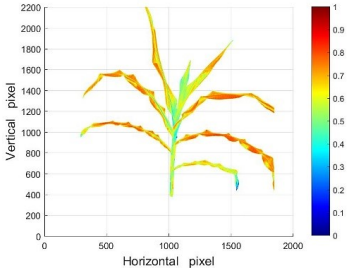

(i) 30°-N-deficiency

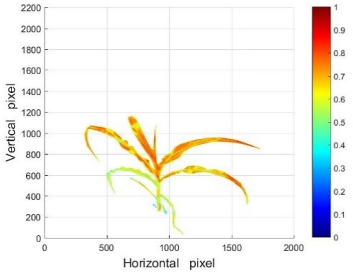

(j) 45°-drought

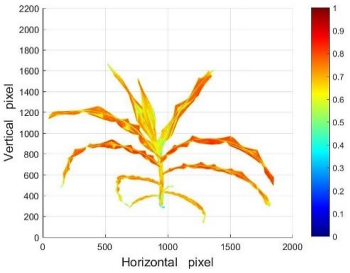

(k) 45°-control

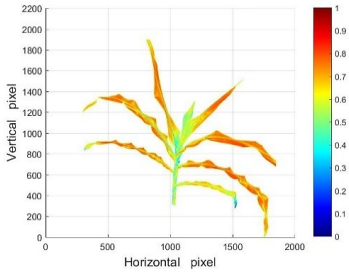

(l) 45°-N-deficiency

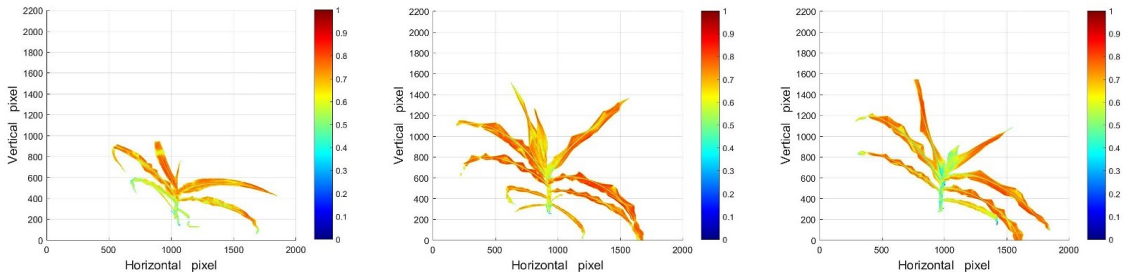

(m) 60°-drought (n) 60°-control (o) 60°-N-deficiency

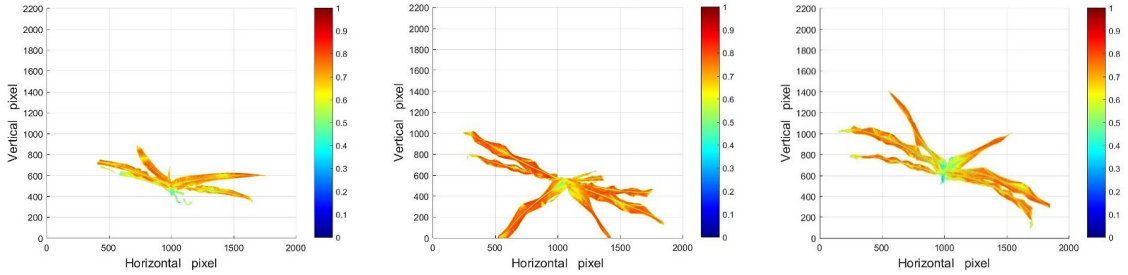

(p) 75°-drought (q) 75°-control (r) 75°-N-deficiency

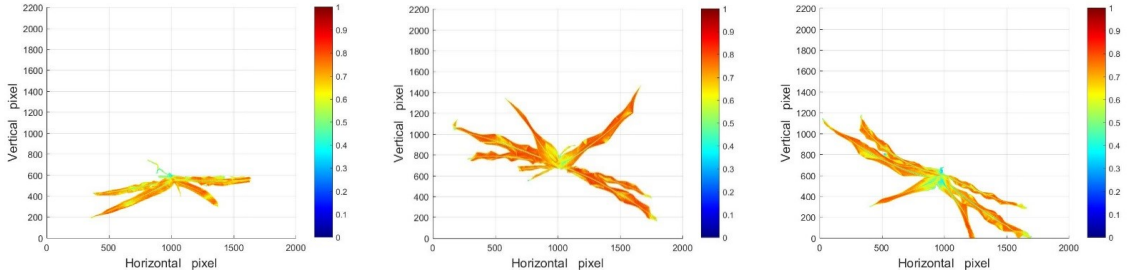

(s) 90°-drought (t) 90°-control (u) 90°-N-deficiency

Fig. 3.3. Colormaps of pixel NDVI of 3 corn plants in 3 different treatments at different imaging angles from side view to top view (Note: x-axis means horizontal pixel number and y-axis means perpendicular pixel number)

To quantify the differences of NDVI distributions in two comparative pairs at different imaging angles, the Bhattacharyya distance (Cha and Srihari, 2002) was applied. It measures the similarity of two discrete or continuous probability distri-

butions. In this study, histograms were used to obtain discrete probability distributions. For discrete probability distributions p and q over the same domain X, the Bhattacharyya distance is defined below (eq. 3.2 & eq. 3.3):

$$BC(p,q) = \sum_{x \in X} \sqrt{p(x)q(x)} \tag{3.2}$$

$$D_B(p,q) = -\ln(BC(p,q)) \tag{3.3}$$

Where, BC is the Bhattacharyya coefficient for discrete probability distributions, and D_B is the Bhattacharyya distance between the two probability distributions p and q.

By computing histograms over the same domain, discrete probability distribution of pixel NDVI was generated for each plant. For plants in each treatment, their probability distributions were averaged as one distribution. At different imaging angles, these averaged probability distributions were compared, and the Bhattacharyya distances were calculated in two comparative pairs. In the bar chart of Bhattacharyya distances of pixel-level NDVI distributions in 2 comparative pairs at different imaging angles (Fig. 3.4), x-axis is the imaging angles from side view to top view with an interval of 15°, and y-axis stands for the Bhattacharyya distances. The difference is bigger when the Bhattacharyya distance is larger. The trends, showed in Fig. 3.4, are almost consistent with that from the t-test result of plant-level NDVI (Fig. 3.2). However, in Fig. 3.4, Pair 1 has the biggest Bhattacharyya distance at 75°, while, Pair 2 has the biggest Bhattacharyya distance at 15°. It's explicit that the imaging

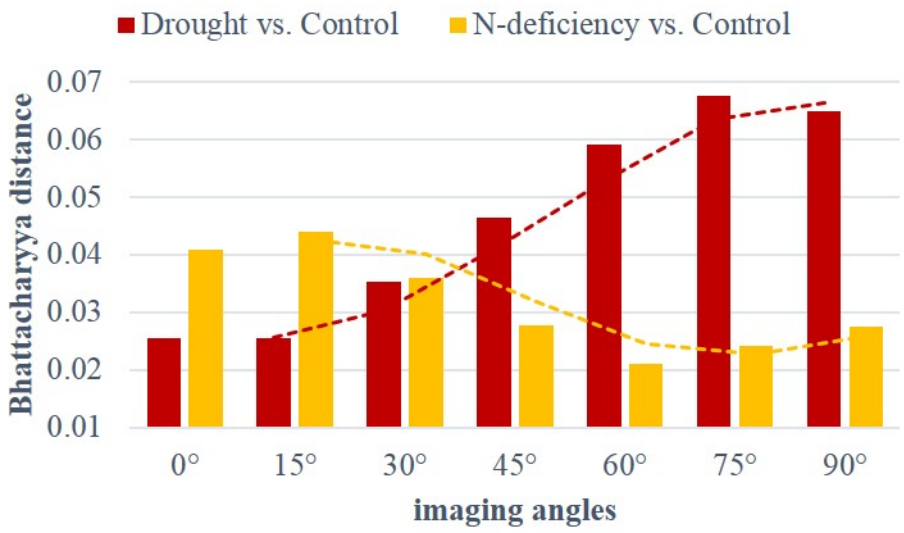

Fig. 3.4. Bar chart of Bhattacharyya distances of pixel-level NDVI distributions in 2 comparative pairs at different imaging angles from side view to top view

angle a little bit tilted from top view is optimized to compare NDVI difference between different water treatments, and the imaging angle a little bit tilted from side view is optimized to tell NDVI difference between different N treatments.

3.2 RWC distribution

As described in Chapter 2, the relative water content (RWC) is another important index for plant phenotyping. To compare RWC conditions at different imaging angles, the plants in the drought-stressed group and control group (Pair 1) were selected. In this study, we focus on RWC distributions on the whole plants instead of just representing RWC of one plant with one average value. To achieve this,

partial least square regression (PLSR), one of the reliable analytical tools for modeling, was applied to predict the relative water content of each pixel on the plants. First of all, PLSR models were built at each imaging angle using the average spectra of plants (independent variables) and the ground truth measurements (dependent variables). Because of properties of the hyperspectral camera sensor and lighting source, 450∼900 nm wavelengths were picked to decrease the noise. To avoid overfitting, rigorous validation is necessary (Westerhuis et al., 2008). The leave-one-out method, using an entire model to fit all the data except a single point, was applied to cross validate the prediction models. It's one of the most powerful cross-validation methods (Yu et al., 2014). The cross-validation R squares of these PLSR models from 0° to 90° are 0.898, 0.925, 0.954, 0.923, 0.937, 0.937 and 0.929, respectively. From this point of view, 30° has the optimized PLSR fitting to the ground truth RWC measurements. Then, at each imaging angle, RWC of each pixel was predicted using the corresponding PLSR model developed above. Histograms and Bhattacharyya distances were repeated to illustrate pixel-level RWC distribution distributions on the corn plants and to compare the differences in Pair 1 at different imaging angles.

Using the same method of pixel-level NDVI distribution analysis, probability distribution of pixel-level RWC distribution was generated for each plant in Pair 1 at each imaging angle. To decrease the noise and improve the accuracy, we removed outliers of predicted pixel-level RWC distribution for each plant. Because the PLSR models were developed based on RWC of top-collar leaves, the prediction values of uppermost leaves with more water contents could be larger than 100%, while, the

prediction values of very bottom leaves or stems with much less water contents could be smaller than 0. In this study, we focus on RWC distributions on the whole plants and distribution differences at different imaging angles instead of precisely predicting all the pixel-level RWC values.

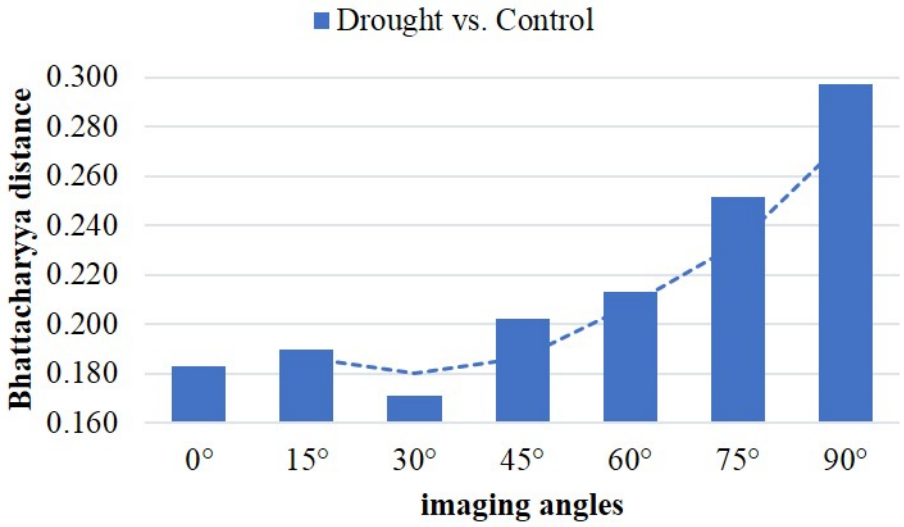

Fig. 3.5. Bar chart of Bhattacharyya distances of pixel-level RWC distributions between the drought-stressed group and control group at different imaging angles from side view to top view

According to the prediction results, the range from -50 to 250 was opted as the comparison domain between the drought-stressed group and control group at different imaging angles. For each treatment, all the probability distributions were averaged as one distribution, and then these averaged distributions were compared at different imaging angles. In the bar chart of Bhattacharyya distances of pixel-level RWC distributions in Pair 1 at different imaging angles (Fig. 3.5), x-axis is

the imaging angles from side view to top view with an interval of 15°, and y-axis stands for the Bhattacharyya distances. The larger distance means bigger difference between these two groups. The approximate trend is that the distance increases with the imaging angle rising from 0° to 90°. Therefore, higher imaging angles are better to tell pixel-level RWC distribution differences, which is consistent with the conclusion from the NDVI comparison of different water treatments.

4. CONCLUSIONS

According to the PROSAIL model, leaf reflectance spectra change at different imaging angles, leading to indices (e.g. NDVI) inconsistent at differential angles. However, current plant phenotyping platforms only focus on top view or side view. In this study, a swing hyperspectral imaging tower that enables us to rotate the camera and lighting source to capture images of plants at any imaging angle from side view (0°) to top view (90°) was designed and built; a randomized block design with 36 corn plants in 3 different treatments (high N and drought-stressed, high N and well-watered, N-deficiency and well-watered) was implemented; hyperspectral images of these corn plants were captured at 7 angles with an interval of 15°, and these images were processed using algorithms developed; optimized imaging angles for NDVI and RWC indices were determined by means of statistical analysis.

For averaged NDVI through all the pixel on each plant (plant-level NDVI), between the drought-stressed group and control group (Pair 1), the difference is becoming larger at higher imaging angles (near to top view); meanwhile, between the N-deficiency group and control group, the difference is becoming larger at lower imaging angles (near to side view). For pixel-level NDVI distribution, it's more explicit that the imaging angle a little bit tilted from top view is optimized to compare NDVI

difference between different water treatments, while, the imaging angle a little bit tilted from side view is optimized to tell NDVI distribution difference between different N treatments. For pixel-level RWC distribution, higher imaging angles (close to top view) are better to tell the RWC distribution difference between different water treatments.

In conclusion, higher imaging angles (close to top view) are better to tell NDVI and RWC differences between the drought-stressed and control groups, while, lower imaging angles (close to side view) are better to tell the NDVI difference between the N-deficiency and control groups. In other words, higher imaging angles (close to top view) are more suitable to separate different water treatments, while, lower imaging angles (close to side view) are more suitable to separate different N treatments.

5. RECOMMENDATIONS

This study shows that optimized imaging angles are different for different N and water treatments. The higher imaging angles (close to top view) are better to separate different water treatments, and the lower imaging angles (close to side view) are better to separate different N treatments. Therefore, researchers need to adjust the imaging modes (side view or top view) according to the treatments applied on experimental samples. In this study, we only focus on corn plants at V7 and V8 stages. For other species, more experiments should be implemented.

REFERENCES

REFERENCES

Abendroth, L.J., Elmore, R.W., Boyer, M.J., Marlay, S.K. (2011). Corn growth and development. Iowa State University Extension Publication, #PMR-1009. Available online at <https://store.extension.iastate.edu/Product/Corn-Growth-and-Development>.

Baresel, J.P., Rischbeck, P., Kipp, S., Barmeier, G., Schmidhalter, U., Hu, Y.C., Mistele, B. (2017). Use of a digital camera as alternative method for non-destructive detection of the leaf chlorophyll content and the nitrogen nutrition status in wheat. Computers and Electronics in Agriculture, 140, 25-34.

Behmann, J., Acebron, K., Emin, D., Bennertz, S., Matsubara, S., Thomas, S., Bohnenkamp, D., Kuska, M.T., Jussila, J., Salo, H., Mahlein, A.K., Rascher, U. (2018). Specim IQ: evaluation of a new, miniaturized handheld hyperspectral camera and its application for plant phenotyping and disease detection. Sensors, 18(2), 441. https://doi.org/10.3390/s18020441

Cha, S.H., Srihari, S.N. (2002). On measuring the distance between histograms. Pattern Recognition, 35(6), 1355-1370.

Collins, W. (1978). Remote sensing of crop type and maturity, Photogrammetric Engineering and Remote Sensing, 44, 43-55.

Dhondt, S., Wuyts, N., Inz, N. (2013). Cell to whole-plant phenotyping: the best is yet to come. Trends in Plant Science, 18(8), 428-439.

Elvidge, C.D., Chen, Z.K. (1995). Comparison of broad-band and narrow-band red and near-infrared vegetation indices. Remote Sensing of Environment, 54(1), 38-48.

Enciso, J., Maeda, M., Landivar, J., Jung, J.H., Chang, A.J. (2017). A ground based platform for high throughput phenotyping. Computers and Electronics in Agriculture, 141, 286-291.

Fahlgren, N., Gehan, M.A., Baxter, I. (2015). Lights, camera, action: high-throughput plant phenotyping is ready for a close-up. Plant Biology, 24, 93-99.

Fiorani, F., Schurr, U. (2013). Future Scenarios for Plant Phenotyping. Annual Review of Plant Biology, 64(1), 267-291.

Granier, C., Aguirrezabal, L., Chenu, K., Cookson, S., Dauzat, M., Hamard, P., Tardieu, F. (2006). PHENOPSIS, an automated platform for reproducible phenotyping of plant responses to soil water deficit in Arabidopsis thaliana permitted the identification of an accession with low sensitivity to soil water deficit. New Phytologist, 169(3), 623-635.

Hartmann, A., Czauderna, T., Hoffmann, R., Stein, N., Schreiber, F. (2011). HTPheno: An image analysis pipeline for high-throughput plant phenotyping. BMC Bioinformatics, 12(1), 148-157.

Jackson, R., Slater, P., Pinter, P. (1983). Discrimination of growth and water stress in wheat by various vegetation indices through clear and turbid atmospheres. Remote Sensing of Environment, 13(3), 187-208.

Jacquemoud, S., Baret, F. (1990). PROSPECT: A model of leaf optical properties spectra. Remote Sensing of Environment, 34(2), 75-91.

Jacquemoud, S., Verhoef, W., Baret, F., Bacour, C., Zarco-Tejada, P.J., Asner, G.P., Francois, C., Ustin, S.L. (2009). PROSPECT+SAIL models: A review of use for vegetation characterization. Remote Sensing of Environment, 113(1), S56-S66.

Klukas, C., Chen, D.J., Pape, J.M. (2014). Integrated analysis platform: an open-source information system for high-throughput plant phenotyping. Plant Physiology, 165(2), 506-518.

Lei, Y.B., Yin, C.Y., Li, C.Y. (2006). Differences in some morphological, physiological, and biochemical responses to drought stress in two contrasting populations of Populus przewalskii. Physiologia Plantarum, 127(2), 182-191.

Li, L., Zhang, Q., Huang, D.F. (2014). A review of imaging techniques for plant phenotyping. Sensors, 14(11), 20078-20111.

Matin, M., Brown, J., Ferguson, H. (1989). Leaf water potential, relative water-content, and diffusive resistance as screening techniques for drought resistance in barley. Agronomy Journal, 81(1), 100-105.

Nagel, K.A., Putz, A., Gilmer, F., Heinz, K., Fischbach, A., Pfeifer, J., Faget, M., Blossfeld, S., Ernst, M., Dimaki, C., et al (2012). GROWSCREEN-Rhizo is a novel phenotyping robot enabling simultaneous measurements of root and shoot growth for plants grown in soil-filled rhizotrons. Functional Plant Biology, 39(11), 5-6.

Pagola, M., Ortiz, R., Irigoyen, I., Bustince, H., Barrenechea, E., Aparicio-Tejo, P., Lamsfus, C., Lasa, B. (2009). New method to assess barley nitrogen nutrition status based on image colour analysis: Comparison with SPAD-502. Computers and Electronics in Agriculture, 65(2), 213-218.

Pimentel, D., Hepperly, P., Hanson, J., Douds, D., Seidel, Rita. (2005). Environmental, energetic, and economic comparisons of organic and conventional farming systems. BioScience, 55(7), 573-582.

Rahaman, Md.M., Chen, D.J., Gillani, Z., Klukas, C., Chen, M. (2015). Advanced phenotyping and phenotype data analysis for the plant growth and development study. Frontiers in Plant Science, 6, 619. https://doi.org/10.3389/fpls.2015.00619

Reyes, J.F., Correa, C., Ziga, J. (2017). Reliability of different color spaces to estimate nitrogen SPAD values in maize. Computers and Electronics in Agriculture, 143, 14-22.

Sadok, W., Naudin, P., Boussuge, B., Muller, B., Welcker, C., Tardieu, F., (2007). Leaf growth rate per unit thermal time follows QTL-dependent daily patterns in hundreds of maize lines under naturally fluctuating conditions. Plant Cell Environ, 30(2), 135-146.

Salas, E., Henebry, G. (2014). A new approach for the analysis of hyperspectral data: Theory and sensitivity analysis of the moment distance method. Remote Sensing, 6(1), 20-41.

Schaepman-Strub, G., Schaepman, M.E., Painter, T.H., Dangel, S., Martonchik, J.V. (2006). Reflectance quantities in optical remote sensingdefinitions and case studies. Remote Sensing of Environment, 103(1), 27-42.

Sharma, P.K., Tiwari, G.N., Sorayan, V.P.S. (1999). Temperature distribution in different zones of the micro-climate of a greenhouse: A dynamic model. Energy Conversion and Management, 40(3), 335-348.

Sumner, M.E. (1977). Application of Beaufils' diagnostic indices to maize data published in the literature irrespective of age and conditions. Plant and Soil, 46(2), 359-369.

Tester, M., Langridge, P. (2010). Breeding technologies to increase crop production in a changing world. Science, 327(5967), 818-822.

Tucker, C.J. (1979). Red and photographic infrared linear combination for monitoring vegetation. Remote Sensing of Environment, 8, 127-150.

Turner, N. (1981). Techniques and experimental approaches for the measurement of plant water status. Plant and Soil, 58(1), 339-366.

Walter, A., Scharr, H., Gilmer, F., Zierer, R., Nagel, K., Ernst, M., Schurr, U. (2007). Dynamics of seedling growth acclimation towards altered light conditions can be quantified via GROWSCREEN: A setup and procedure designed for rapid optical phenotyping of different plant species. New Phytologist, 174(2), 447-455.

Westerhuis, J., Hoefsloot, H., Smit, S., Vis, D., Smilde, A., Velzen, E., Duijnhoven, J., Dorsten, F. (2008). Assessment of PLSDA cross validation. Metabolomics, 4(1), 81-89.

Xiong, X., Yu, L.J., Yang, W.N., Liu, M., Jiang, N., Wu, D., Chen, G.X., Xiong, L.Z., Liu, K.D., Liu, Q. (2017). A high-throughput stereo-imaging system for quantifying rape leaf traits during the seedling stage. Plant Methods, 13, 7. https://doi.org/10.1186/s13007-017-0157-7

Yu, K.Q., Zhao, Y.R., Li, X.L., Shao, Y.N., Liu, F., He, Y. (2014). Hyperspectral imaging for mapping of total nitrogen spatial distribution in pepper plant. PLoS One, 9(12), E116205.

Yuan, Z.F., Cao, Q., Zhang, K., Ata-UI-Karim, S.T., Tian, Y.C., Zhu, Y., Cao, W.X., Liu, X.J. (2016). Optimal leaf positions for chlorophyll meter measurement in rice. Frontiers in Plant Science, 7, 719. https://doi.org/10.3389/fpls.2016.00719